A Finite Element Approach to Feynman Diagrams

A Major Qualifying Project Report

Submitted to the Faculty of the

WORCESTER POLYTECHNIC INSTITUTE

In partial fulfillment of the requirements for the

Degree of Bachelor of Science

in Physics

By

Muping Chen

March 22, 2017

Major Project Advisor: Professor L. Ramdas Ram-Mohan

Abstract

Feynman diagrams are essential tools used in the quantum field theory approach to condensed matter problems. It is typical to represent diagrammatic techniques in momentum space assuming implicitly that we have an infinite domain at hand. However, in finite nanoscale systems the momentum is not well-defined, so that the theory has to be reformulated. We espouse the coordinate space description, with the formalism having to satisfy geometric constraints of the physical domain. We show that the finite element method (FEM) is well suited for the quantum field theoretic modeling of nanoscale systems. The FEM uses a discretized physical domain that is faithful to the geometry at hand, and the wavefunctions are solved using a discretized form of the action and its variation.

Acknowledgments

I would like to thank my project advisor, Prof. Ram-Mohan, for suggesting this project and guidance through the whole process. I wish to thank WPI for a Summer Undergraduate Research Fellowship, and Sathwik Bharadwaj for discussion.

Contents

List of Figures

1 Introduction

Quantum field theory provides a systematic approach to the perturbative inclusion of the effects of interactions between fields. Its successes in quantum electrodynamics and quantum chromodynamics are based on the use of Green's functions (GF), or Feynman propagators, to account for the inhomogeneous terms in equations of motion in the presence of interacting quantum fields. The interaction terms lead to nonlinear coupling that in principle demands a solution to all orders.

In general, terms from higher order perturbation theory have complicated expressions. However, Feynman developed a convenient and intuitive diagrammatic representation of those terms which can be easily and visually understood.[1,2] Feynman diagrams show the different paths that particles can follow while transiting from one particular state to another as the system evolves from the initial state to the final state. The collection of all possible paths gives the exact GF, which represents the transition amplitude from one state to another. In typical treatments of quantum field theory and the development of Feynman diagrams,[3–5] it is assumed that the physical system is over an infinite domain, so that particle states can be represented as eigenstates of momentum. The equations of motion satisfied by the quantized fields have inhomogeneous terms arising from the interaction between fields. In momentum space the lowest order propagators are derivable in a very straightforward manner. The higher order corrections to propagators are also expressible in momentum space by using Feynman rules at the one-loop level[3,6,7] to account for virtual excitations in the intermediate states leading to self-energy corrections.

In view of the interest in modeling finite domains at the nanoscale it becomes necessary to employ alternative descriptions to the momentum space approach. In particular, we consider the real space description for the propagators and Feynman diagrams of higher order perturbations. For this purpose, we employ the finite element method (FEM).[8] The FEM is a numerical method for simplifying the geometric constraints in physical problems. The finite element approach uses a discretized physical domain that is faithful to the geometry at hand. The wavefunctions are obtained using a discretized form of the action integral and its variation. It enjoys the advantages of variational (stationary action) analysis for eigenvalues and eigenfunctions in domains with arbitrary geometries where the method provides a systematic approach to improving the accuracy of the results. The real space representation of the Feynman propagators and the higher order loop diagrams lends itself to this discretization in nanoscale systems in a natural manner. It is applicable to higher-order perturbative and nonlinear effects.

By discretizing the domain in order to solve for eigenfunctions and eigenvalues of the excitations in the system. We can construct the lowest order discretized version of the GF. By representing the Feynman diagrams in the framework of FEM, we substantially simplify the issue of solving for eigenfunctions on complex domains. The FEM is very effective in tackling boundary conditions of any type including mixed Dirichlet, Neumann or Cauchy boundary conditions. Calculations can be performed on each element without concerning ourselves about the entire physical domain. This "divide and conquer" approach additionally simplifies the calculations because the behavior of any function in each element is

approximated by specific polynomials chosen by us. The spatial integrals can be immediately performed so that the GFs are expressible in terms of bilinear combinations of the nodal values alone. The complete result can be obtained by summing up the contribution from each element in the discretized domain while we ensure continuity conditions at the inter-element level. The eigenfunctions and eigenvalues are subsequently used in the determination of other quantities of interest, such as the lowest order propagator, the self-energy and vertex corrections.

The freedom to consider any type of boundary condition has the advantage that we can directly obtain wavefunctions that are consistent with derivative boundary conditions or mixed boundary conditions as are needed in scattering theory and carrier transport.[8]

In Sec. 2 we begin by very briefly reviewing the standard theory of propagators and one-loop diagrams for the infinite domain. In Sec. 4 this is followed by the development of the same theory over a finite domain. A final overview is given in concluding remarks in Sec. 5 .

2 Feynman diagrams for the infinite domain

a Lowest order propagators

We begin by reviewing very briefly the derivation of Feynman propagators for the infinite domain. For the moment, we consider particle excitations above the ground state, $|0\rangle$, which is the vacuum state in field theory.[3,6,7] This is readily generalized to the case of the many-body ground state, $|\Psi_0\rangle$.[9–11]

The initial state at $t=-\infty$ evolves with time to its final state at $t=\infty$. This evolution is generated by the time evolution operator $U(\infty,-\infty)$ acting on the initial state. The single particle GF defined in coordinate space takes the form

$$\begin{aligned} iG_{\alpha\beta}(x,x') &= \langle 0|T[\hat{\psi}_{H\alpha}(x)\hat{\psi}^{\dagger}_{H\beta}(x')]|0\rangle \\ &= \frac{\langle 0|T[\hat{\psi}_{I\alpha}(x)\hat{\psi}^{\dagger}_{I\beta}(x')U(\infty,-\infty)]|0\rangle}{\langle 0|U(\infty,-\infty)|0\rangle}. \end{aligned} \tag{1}$$

Here $x=(\mathbf{x},t)$, and the operators $\hat{\psi}_{H\alpha}(x)$ and $\hat{\psi}_{I\alpha}(x')$ are the Heisenberg and Interaction picture field operators, respectively. defined in the Heisenberg picture, with the first being the annihilation operator and the second one is the creation operator. The second one is the definition in interaction picture. With these definitions, the GF defined in Eq. (1) gives the probability amplitude of creating a particle at x' and annihilating it at x, in the physical ground state. The time evolution operator U allows us to take matrix elements in the same basis. The time-ordering of fields denoted by T is included in order to make the expression compatible with the causal nature of this evolution. It is useful to recognize that only the terms representing connected Feynman diagrams from the numerator will survive since the denominator cancels the terms corresponding to the disconnected diagrams. With these simplifications we write

$$iG_{\alpha\beta}(x,x') = \langle 0|T[\hat{\psi}_{I\alpha}(x)\hat{\psi}^{\dagger}_{I\beta}(x')U(\infty,-\infty)]|0\rangle_{\text{conn.}}. \tag{2}$$

Since the evolution operator can be expressed as

$$\hat{U}(t,t') = T\{\exp\left[-i\hbar^{-1}\int_t^{t'} dt_1 \hat{H}_I(t_1)\right]\}, \tag{3}$$

the GF takes the form

$$\begin{aligned} iG(x,x') &= \sum_n \left(\frac{1}{i\hbar}\right)^n \frac{1}{n!}\int_{-\infty}^{\infty} dt_1 \cdots \int_{-\infty}^{\infty} dt_n \\ &\times \langle 0|T[\hat{H}_I(t_1)\cdots\hat{H}_I(t_n)\hat{\psi}(x)\hat{\psi}^\dagger(x')]|0\rangle_{\text{conn.}}. \end{aligned} \tag{4}$$

From now on, the system is assumed to be spin independent so that the spin indices will be suppressed. Also, since we shall continue working in the interaction picture, the subscript "I" is suppressed. The field operators in the interaction picture are related to field operators in the Schrödinger picture by

$$\left\{ \begin{array}{c} \hat{\psi}(x) \\ \hat{\psi}^\dagger(x) \end{array} \right\} = \left\{ \begin{array}{l} e^{i\hat{H}_0 t/\hbar}\hat{\psi}(\mathbf{x})\ e^{-i\hat{H}_0 t/\hbar} \\ e^{i\hat{H}_0 t/\hbar}\hat{\psi}^\dagger(\mathbf{x})e^{-i\hat{H}_0 t/\hbar} \end{array} \right\}. \tag{5}$$

Here, $\hat{\psi}(\mathbf{x})$ and $\hat{\psi}^\dagger(\mathbf{x})$ are the field operators in the Schrödinger picture, and are related to the lowering and raising operators by

$$\begin{aligned} \hat{\psi}(\mathbf{x}) &= \sum_a \psi_a(\mathbf{x})c_a, \\ \hat{\psi}^\dagger(\mathbf{x}) &= \sum_b \psi_b(\mathbf{x})c_b^\dagger, \end{aligned} \tag{6}$$

where a, b are sets of quantum numbers. Combining Eq. (5) and Eq. (6), one has the free electron propagator

$$\begin{aligned} iG^{(0)}(x,x') = \sum_n \Big\{ & \theta(t-t')e^{-i\omega_n(t-t')} \\ & \times \langle 0|\hat{\psi}(\mathbf{x})|n\rangle\langle n|\hat{\psi}^\dagger(\mathbf{x}')|0\rangle \\ & -\theta(t'-t)e^{i\omega_n(t'-t)} \\ & \times \langle 0|\hat{\psi}^\dagger(\mathbf{x}')|n\rangle\langle n|\hat{\psi}(\mathbf{x})|0\rangle \Big\}. \end{aligned} \tag{7}$$

For the moment, in order to be brief, we can focus on the retarded GF since the advanced GF and the Feynman GF can be derived from it. Fourier transforming the first term in Eq. (7) to frequency space, the retarded GF is given by

$$iG^{R,0}(\mathbf{x},\mathbf{x}',\omega) = \sum_n \frac{\langle 0|\hat{\psi}(\mathbf{x})|n\rangle\langle n|\hat{\psi}^\dagger(\mathbf{x}')|0\rangle}{\omega - \omega_n + i\eta}. \tag{8}$$

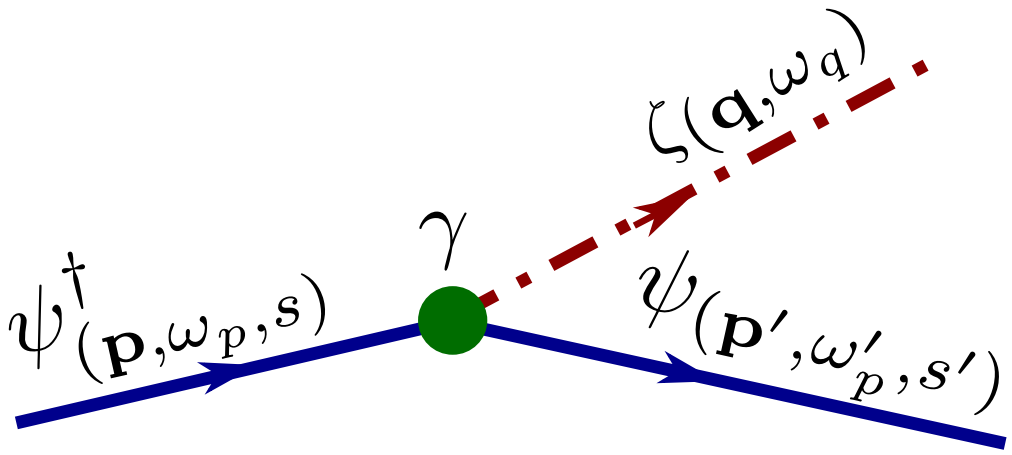

Figure 1: The first order phonon emission diagram is shown for an infinite system. The incoming electron has momentum and spin (p, s), while the outgoing electron has (p', s'). The emitted phonon has wavevector and frequency of $(\mathbf{q}, \omega_q)$.The coupling is $\gamma = e$. The phonon field has a derivative coupling with the electrons, and the Fröhlich interaction parameters are included in the field $\zeta(q, \omega_q)$ for convenience.

Before considering the perturbative expansion of the exact GF in detail, it is useful to investigate the infinite space with translational symmetry, where the GF depends on the spatial displacement $\mathbf{x} - \mathbf{x}'$. Now Eq. (8) can be rewritten as

$$iG^{R,0}(\mathbf{x}-\mathbf{x}'\,\omega)=\sum_n \frac{\langle 0|\hat{\psi}(0)|n\rangle\langle n|\hat{\psi}^\dagger(0)|0\rangle e^{i\mathbf{k}_n\cdot(\mathbf{x}-\mathbf{x}')}}{\omega-\omega_n+i\eta},$$

where $E_n = \hbar\omega_n$ has been used. Fourier transforming this equation into $(\mathbf{k}, \omega)$ space we obtain

$$iG^{R,0}(\mathbf{k},\omega)=\sum_n V\frac{\langle 0|\hat{\psi}(0)|n\rangle\langle n|\hat{\psi}^\dagger(0)|0\rangle}{\omega-\omega_n+i\eta}\delta_{\mathbf{k},\mathbf{k}_n}. \tag{9}$$

The significance of the Kronecker-delta is that for each state n, there is a corresponding wavevector $\mathbf{k}$; therefore, each state can be represented by $\mathbf{k}$. Inserting the wavevector $\mathbf{k}$ into the expression, one obtains

$$iG^{R,0}(\mathbf{k},\omega) = V\frac{\langle 0|\hat{\psi}(0)|\mathbf{k}\rangle\langle \mathbf{k}|\hat{\psi}^\dagger(0)|0\rangle}{\omega-\omega_{\mathbf{k}}+i\eta}. \tag{10}$$

3 Phonon emission and self-energy

a Phonon emission

Consider the Frölich coupling of electrons with lattice vibrations in polar materials. The electron-phonon coupling is given by

$$H_I = \gamma\int d^3x\,\hat{\psi}^\dagger(x)\hat{\psi}(x)\,\hat{\zeta}(x). \tag{11}$$

Here the gradient of the atomic displacement field $\mathbf{W}(\mathbf{r},t)$ is represented by $\zeta(x)$.

The transition amplitude for $e(\mathbf{k}_i) \rightarrow e(\mathbf{k}_f) + \zeta(\mathbf{q}_i)$ is given by the lowest order perturbation term

$$\begin{aligned} S_{fi} &= \frac{-i}{\hbar}\langle \mathbf{k}_f, \mathbf{q}|\gamma \int d^3r\, dt \mathcal{H}_I|\mathbf{k}_i\rangle \\ &= \frac{-i\gamma}{\hbar} 2\pi\delta(\omega_{k_i} - \omega_{k_f} - \omega_q)\, \Lambda \int d^3r e^{i(\mathbf{k}_i - \mathbf{q} - \mathbf{k}_f)\cdot\mathbf{r}} \\ &= \frac{-i\gamma}{\hbar}\Lambda(2\pi)^4\delta(\omega_{k_i} - \omega_q - \omega_{k_f})\delta(\mathbf{k}_i - \mathbf{q} - \mathbf{k}_f). \end{aligned} \tag{12}$$

The transition rate per unit time per unit interaction volume can now be calculated in the usual manner by integrating $|S_{fi}|^2$ over available phase space for the particles in the final state. We have

$$\begin{aligned} \mathcal{R}_{fi} &= \frac{1}{2}\sum_{spins}\frac{|S_{fi}|^2}{VT} \\ &= \frac{2\gamma^2\Lambda^2}{\hbar^2}(2\pi)^4\delta^{(4)}(k_i - q - k_f)G_{fi}. \end{aligned} \tag{13}$$

Here G_{fi} is the overlap function for the initial and final electron states. The resulting linewidth is given by

$$\Gamma_{\text{emission}} = V^2 \int \frac{d^3q}{(2\pi)^3}\int \frac{d^3k_f}{(2\pi)^3}\mathcal{R}_{fi},$$

corresponding to 1 incoming particle in volume V.

b The self-energy diagram

For the second order contribution shown in Fig. 2, we write %%

$$\begin{aligned} iG^{(2)}(x,x') &= \frac{-1}{2\hbar^2}\int d^4x_1 d^4x_2 \\ &\quad \times\langle 0|T\left[\hat{\psi}(x)\hat{\psi}^\dagger(x') :\hat{H}_I(x_2)::\hat{H}_I(x_1):\right]|0\rangle. \end{aligned} \tag{14}$$

Expressed in terms of single-particle Green's functions we have

$$\begin{aligned} iG^{(2)}(x,x') &= \frac{-\gamma^2}{2\hbar^2}\int d^4x_1 d^4x_2 \\ &\quad \times\langle 0|T\Big[\left(\hat{\psi}(x)\hat{\psi}^\dagger(x_2)\right)\left(\hat{\psi}(x_2)\hat{\psi}^\dagger(x_1)\right) \\ &\quad \times\left(\hat{\psi}(x_1)\hat{\psi}^\dagger(x')\right)\left(\hat{\zeta}(x_2)\hat{\zeta}(x_1)\right)\Big]|0\rangle, \\ &= \frac{-\gamma^2}{2\hbar^2}\int d^4x_1 d^4x_2\, G^{(0)}(x - x_2)G^{(0)}(x_2 - x_1) \\ &\qquad \times\tilde{D}^{(0)}(x_2 - x_1)G^{(0)}(x_1 - x'). \end{aligned} \tag{15}$$

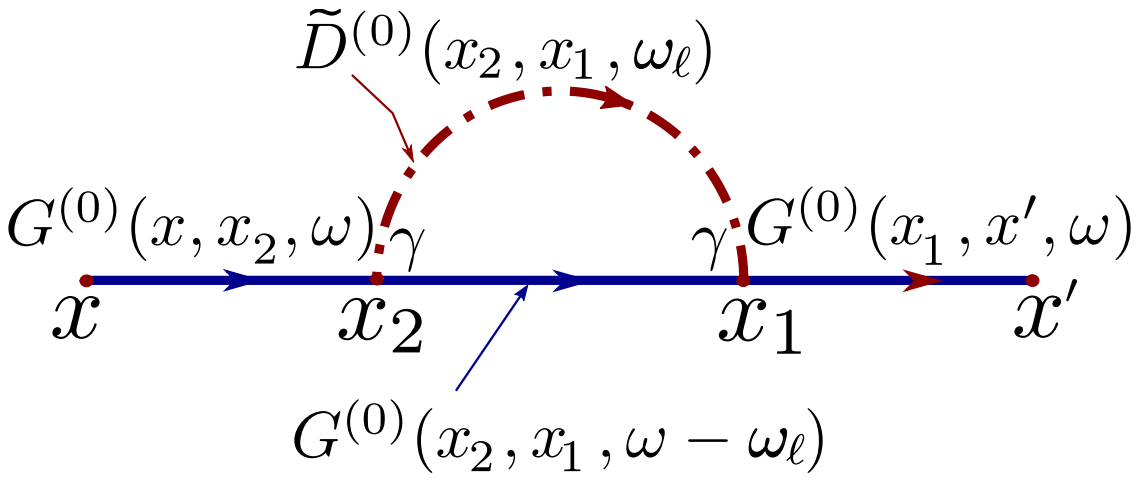

Figure 2: The second order self-energy diagram $G^{(2)}(\mathbf{x}, \mathbf{x}', \omega)$ of the electron-phonon interaction is shown for an infinite system.

For illustrative purposes, we have retained only the one loop electron-LO phonon self-energy diagram while dropping the "tadpole" diagram that also appears in the second order.

The GF can be Fourier expanded in frequency space as

$$iG(x, x') = i \int \frac{d\omega}{2\pi} e^{-i\omega(t-t')} G(\mathbf{x} - \mathbf{x}', \omega). \tag{16}$$

Using this relation, Eq. (14) can be recast as

$$\begin{aligned} iG^{(2)}(x, x') &= \frac{-\gamma^2}{2\hbar^2} \int d^4x_1 d^4x_2 \int d\omega \, d\omega_1 d\omega_2 d\omega' \\ &\times \frac{1}{(2\pi)^4} e^{-i\omega(t-t_2)} e^{-i\omega_2(t_2-t_1)} e^{-i\omega_1(t_2-t_1)} \\ &\times e^{-i\omega'(t_1-t')} G^{(0)}(\mathbf{x}-\mathbf{x_2}, \omega) G^{(0)}(\mathbf{x_2}-\mathbf{x_1}, \omega_1) \\ &\times \tilde{D}^{(0)}(\mathbf{x_2}-\mathbf{x_1}, \omega_2) G^{(0)}(\mathbf{x_1}-\mathbf{x}', \omega'), \end{aligned} \tag{17}$$

Integrating over time variables we have

$$\begin{aligned} iG^{(2)}(x, x') &= \frac{-\gamma^2}{2\hbar^2} \int d^4x_1 d^4x_2 \int d\omega d\omega_1 \frac{e^{-i\omega t + i\omega' t'}}{4\pi^2} \\ &\times G^{(0)}(\mathbf{x}-\mathbf{x_2}, \omega) G^{(0)}(\mathbf{x_2}-\mathbf{x_1}, \omega_1) \tilde{D}^{(0)}(\mathbf{x_2}-\mathbf{x_1}, \omega_2) \\ &\times G^{(0)}(\mathbf{x_1}-\mathbf{x}', \omega') \delta(\omega_1+\omega_2-\omega) \delta(\omega'-\omega_1-\omega_2). \end{aligned} \tag{18}$$

The last factors in the equation are the δ-functions associated with energy conservation at

each vertex. Collecting terms, Eq. (18) can be rewritten as

$$\begin{aligned} iG^{(2)}(x,x') &= \int \frac{d\omega}{2\pi}\, e^{-i\omega(t-t')}\left[\frac{-\gamma^2}{2\hbar^2}\int d^3x_1 d^3x_2\right. \\ &\quad \times \int \frac{d\omega_1}{2\pi}\, G^{(0)}(\mathbf{x}-\mathbf{x_2},\omega)G^{(0)}(\mathbf{x_2}-\mathbf{x_1},\omega_1) \\ &\quad \left.\times \tilde{D}^{(0)}(\mathbf{x_2}-\mathbf{x_1},\omega-\omega_1)G^{(0)}(\mathbf{x_1}-\mathbf{x}',\omega)\right]. \end{aligned} \tag{19}$$

The factor in square brackets in the above is identified as $G(\mathbf{x}-\mathbf{x}',\omega)$ to the second order in perturbation theory. The Fourier transformation of $iG(\mathbf{x}-\mathbf{x}',\omega)$ is given by

$$iG(\mathbf{x}-\mathbf{x}',\omega) = \frac{i}{(2\pi)^3}\int d^3k\, e^{i\mathbf{k}\cdot(\mathbf{x}-\mathbf{x}')}G(\mathbf{k},\omega). \tag{20}$$

With this relation, we have

$$\begin{aligned} iG^{(2)}(\mathbf{x}-\mathbf{x}',\omega) &= \frac{-\gamma^2}{2\hbar^2}\int d^3x_1 d^3x_2 \int \frac{d\omega_1}{2\pi} \\ &\quad \times \frac{1}{(2\pi)^{12}}\int d^3k\, d^3k_1 d^3k_2 d^3k' e^{i\mathbf{k}\cdot(\mathbf{x}-\mathbf{x_2})} \\ &\quad \times e^{i\mathbf{k}\cdot(\mathbf{x}-\mathbf{x_2})}e^{i\mathbf{k_1}\cdot(\mathbf{x_2}-\mathbf{x_1})}e^{i\mathbf{k_2}\cdot(\mathbf{x_2}-\mathbf{x_1})}e^{i\mathbf{k}'\cdot(\mathbf{x_1}-\mathbf{x}')} \\ &\quad \times G^{(0)}(\mathbf{k},\omega)G^{(0)}(\mathbf{k_1},\omega_1)\tilde{D}^{(0)}(\mathbf{k_2},\omega_2)G^{(0)}(\mathbf{k}',\omega), \end{aligned} \tag{21}$$

with $\omega_2 = \omega - \omega_1$. Integrating over the coordinates $\boldsymbol{x_1}, \boldsymbol{x_2}$, we obtain

$$\begin{aligned} iG(\mathbf{x}-\mathbf{x}',\omega) &= \frac{-\gamma^2}{2\hbar^2}\frac{1}{(2\pi)^{13}}\int d\omega_1 \int d^3k\, d^3k_1 d^3k_2 d^3k' \\ &\quad \times e^{i\mathbf{k}\cdot\mathbf{x}-i\mathbf{k}'\cdot\mathbf{x}'}G^{(0)}(\mathbf{k},\omega)G^{(0)}(\mathbf{k_1},\omega_1)\tilde{D}^{(0)}(\mathbf{k_2},\omega_2) \\ &\quad \times G^{(0)}(\mathbf{k}',\omega)\delta^{(3)}(\mathbf{k_1}+\mathbf{k_2}-\mathbf{k})\delta^{(3)}(\mathbf{k}'-\mathbf{k_2}-\mathbf{k_1}) \\ &= \frac{1}{(2\pi)^3}\int d^3k\, e^{i\mathbf{k}\cdot(\mathbf{x}-\mathbf{x}')}G^{(0)}(k)\left[\frac{-\gamma^2}{2\hbar^2(2\pi)^4}\int d^4k_1\right. \\ &\quad \left.\times G^{(0)}(k_1)\tilde{D}^{(0)}(k-k_1)\right]G^{(0)}(k). \end{aligned} \tag{22}$$

Here, $k = (\mathbf{k},\omega)$, and the delta functions in the intermediate step represent momentum conservation at each vertex. One can also recognize in the square brackets the self-energy

$$i\Sigma^{(2)}(k) = \frac{-\gamma^2}{2\hbar^2}\frac{1}{(2\pi)^4}\int d^4k_1\, G^{(0)}(k_1)\tilde{D}^{(0)}(k-k_1). \tag{23}$$

In polar materials, $\zeta(\mathbf{x}')$ is the phonon field for the electron-phonon coupling. Following the procedure for evaluating a general phonon propagator in momentum space as displayed

in Appendix c , one obtains

$$i\tilde{D}^{(0)}(\mathbf{k},\omega) = \frac{2\pi\hbar\omega_\ell}{ik^2}\left(\frac{1}{\epsilon_\infty}-\frac{1}{\epsilon_0}\right) \times\left[\frac{1}{\omega-\omega_\ell+i\eta}-\frac{1}{\omega+\omega_\ell-i\eta}\right]. \quad (24)$$

Using the (many-body) electron propagator introduced in Appendix e the self-energy term can be written as

$$\Sigma^{(2)}(\mathbf{k},\omega) = \frac{i\gamma^2}{2(2\pi)^3\hbar}\left(\frac{1}{\epsilon_\infty}-\frac{1}{\epsilon_0}\right)\int d^4k_1\frac{\omega_\ell}{|\mathbf{k}-\mathbf{k}_1|^2} \times\left[\frac{1}{\omega-\omega_1-\omega_\ell+i\eta}-\frac{1}{\omega-\omega_1+\omega_\ell-i\eta}\right] \times\left[\frac{\theta(\mathbf{k}_1-\mathbf{k}_F)}{\omega_1-\omega(\mathbf{k}_1)+i\eta}-\frac{\theta(\mathbf{k}_F-\mathbf{k}_1)}{\omega_1-\omega(\mathbf{k}_1)-i\eta}\right]. \quad (25)$$

The integration in ω can be performed by contour integration to obtain

$$\Sigma^{(2)}(\mathbf{k},\omega) = \frac{-\gamma^2}{2\hbar}\left(\frac{1}{\epsilon_\infty}-\frac{1}{\epsilon_0}\right)\int\frac{d^3k_1}{(2\pi)^3}\,\frac{\omega_\ell}{|\mathbf{k}-\mathbf{k}_1|^2} \times\left[\frac{\theta(\mathbf{k}_1-\mathbf{k}_F)}{\omega-\omega(\mathbf{k}_1)-\omega_\ell+i\eta} -\frac{\theta(\mathbf{k}_F-\mathbf{k}_1)}{\omega-\omega(\mathbf{k}_1)+\omega_\ell-i\eta}\right]. \quad (26)$$

The imaginary part of $\Sigma^{(2)}$ is given by

$$\mathrm{Im}\,\Sigma^{(2)}(\mathbf{k},\omega) = \frac{\gamma^2}{2\hbar}\left(\frac{1}{\epsilon_\infty}-\frac{1}{\epsilon_0}\right)\int\frac{d^3k_1}{2(2\pi)^2}\,\frac{\omega_\ell}{|\mathbf{k}-\mathbf{k}_1|^2} \times\Big[\theta(\mathbf{k}_1-\mathbf{k}_F)\delta(\omega-\omega(\mathbf{k}_1)-\omega_\ell) +\theta(\mathbf{k}_F-\mathbf{k}_1)\delta(\omega-\omega(\mathbf{k}_1)+\omega_\ell)\Big]. \quad (27)$$

Let $k_1 = yk_F$, the retarded contribution (from the first δ-function) can be rewritten as

$$\begin{aligned}\mathrm{Im}\,\Sigma^{(2)}(\mathbf{k},\omega) &= C\int\frac{k_F^2y^2dyd\Omega}{(k/k_F)^2+y^2-2ky\cos\theta/k_F} \times\theta(y-1)\delta\left(\omega-\frac{\hbar y^2k_F^2}{2m}-\omega_\ell\right)\\ &= C\int\frac{2m\hbar^{-1}y^2dyd\Omega}{(k/k_F)^2+y^2-2ky\cos\theta/k_F} \times\theta(y-1)\delta(\frac{2m(\omega-\omega_\ell)}{\hbar k_F^2}-y^2), \end{aligned} \quad (28)$$

where we let

$$C = \frac{\gamma^2}{2\hbar}\left(\frac{1}{\epsilon_\infty}-\frac{1}{\epsilon_0}\right)\frac{k_F\omega_\ell}{2(2\pi)^2}. \tag{29}$$

Let us substitute $x=\cos\theta$, $v=y/k_F$; then Eq.(27) can be rewritten as

$$\begin{aligned}\mathrm{Im}\,\Sigma^{(2)}(\mathbf{k},\omega) &= \frac{4\pi mC}{\hbar}\int\frac{y^2dydx}{v^2+y^2-2vyx}\theta(y-1)\\ &\quad\times\delta(\frac{2m(\omega-\omega_\ell)}{\hbar k_F^2}-y^2).\end{aligned} \tag{30}$$

Since $\delta(x^2-a^2)=[\delta(x-a)+\delta(x+a)]/(2a)$, we have

$$\begin{aligned}\mathrm{Im}\,\Sigma^{(2)}(\mathbf{k},\omega) &= \frac{2\pi mC}{\hbar\tilde{\omega}}\int\frac{y^2dydx}{v^2+y^2-2vyx}\theta(y-1)\\ &\quad\times[\delta(\tilde{\omega}-y)+\delta(\tilde{\omega}+y)].\end{aligned} \tag{31}$$

Here, $\tilde{\omega}=2m(\omega-\omega_\ell)/(\hbar k_F^2)$. Performing the y integration first, one obtains

$$\begin{aligned}\mathrm{Im}\,\Sigma^{(2)}(\mathbf{k},\omega) &= \frac{2\pi mC}{\hbar\tilde{\omega}}\int_{-1}^{1}dx\left[\frac{\tilde{\omega}^2\theta(\tilde{\omega}-1)}{v^2+\tilde{\omega}^2-2v\tilde{\omega}x}\right.\\ &\quad\left.+\frac{\tilde{\omega}^2\theta(-\tilde{\omega}-1)}{v^2+\tilde{\omega}^2+2v\tilde{\omega}x}\right]\end{aligned} \tag{32}$$

By elementary integration we get

$$\begin{aligned}\mathrm{Im}\,\Sigma^{(2)}(\mathbf{k},\omega) &= \frac{2\pi mC}{\hbar}\left[\frac{\theta(\tilde{\omega}-1)}{2v}\left(\ln\frac{|v^2+\tilde{\omega}^2+2v\tilde{\omega}|}{|v^2+\tilde{\omega}^2-2v\tilde{\omega}|}\right)\right.\\ &\quad\left.-\frac{\theta(-\tilde{\omega}-1)}{2v}\left(\ln\frac{|v^2+\tilde{\omega}^2-2v\tilde{\omega}|}{|v^2+\tilde{\omega}^2+2v\tilde{\omega}|}\right)\right]\\ &= \frac{2\pi mC}{\hbar}\mathrm{sgn}(\tilde{\omega})\frac{\theta(|\tilde{\omega}|-1)}{2v}\left(\ln\frac{|v^2+\tilde{\omega}^2+2v|\tilde{\omega}||}{|v^2+\tilde{\omega}^2-2v|\tilde{\omega}||}\right).\end{aligned} \tag{33}$$

4 Feynman rules for the finite domain

a Finite element analysis for eigenstates

We first describe the FEM for the evaluation of eigenstates in a given nanoscale system.

In FEM, the physical domain is discretized into subregions called finite elements; within these elements the wavefunction is expressed in terms of the values of the function ψ_{inode} at special points $\mathbf{x}_{inode}$, called nodes in each element, multiplied by interpolation polynomials. The polynomials are chosen such that they can capture the behavior of the wavefunction over individual elements. In other words, in each element iel we write

$$\psi^{(iel)}(\mathbf{x}) = \sum_i \psi_i^{(iel)} N_i^{(iel)}(\mathbf{x}). \tag{34}$$

Here, $N_i,\ i = 1, ...n$ represent the n interpolation polynomials used in each finite element, and the set $\{\psi_i\}$ can include function values (Lagrange elements) as well as derivatives of the interpolated function ψ'_{inode} (Hermite elements). In order to obtain high accuracy we represent the wavefunctions in terms of Hermite interpolation polynomials having $C^{(2)}$-continuity.[8] The wavefunction defined in this manner is valid only within the element *iel* and is zero outside. The full wavefunction is made up by putting together the wavefunctions at the nodes and ensuring continuity across element boundaries. A sum over all the elements can be expressed in terms of a global index α that together identifies the element and the nodal polynomial.

$$\psi(\mathbf{r}) = \sum_{iel} \sum_{i} \psi_i^{iel} N_i^{(iel)}(\mathbf{r}) \equiv \sum_{\alpha} \psi_\alpha N_\alpha(\mathbf{r}). \tag{35}$$

The actual values of the coefficients ψ_α of the interpolation polynomials is determined as follows. We have the action integral that generates the Schrödinger equation on using the principle of stationary action

$$\mathcal{A} \ = \ \int dt \int \psi^\dagger(\mathbf{r}) \left(\overleftarrow{\nabla} \frac{\hbar^2}{2m} \overrightarrow{\nabla} + (V(\mathbf{r}) - E) \right) \psi(\mathbf{r}),$$

with the vector arrows indicating the direction in which the gradient operators act. The discretized form for a time-independent problem is written as

$$\mathcal{A}/T \ = \ \iint d^3r \left(\psi_\alpha^\dagger N_\alpha(\mathbf{r}) \right) \left(\overleftarrow{\nabla} \frac{\hbar^2}{2m} \overrightarrow{\nabla} + V(\mathbf{r}) - E \right) \left(\psi_\beta N_\beta(\mathbf{r}) \right). \tag{36}$$

The horizontal lines through the integral sign are used to indicate that this is an integral discretized over the finite elements.

The integration over space can be performed since the interpolation polynomials have a form chosen by us to work with the discretization. The functional variation with $\psi^\dagger(\mathbf{r})$ is replaced by parameter variation with respect to $\psi_\alpha^\dagger$. The resulting discretized Schrdinger equation is a generalized eigenvalue matrix equation

$$\left(\mathbf{K}_{\alpha\beta} + \mathbf{V}_{\alpha\beta} \right) \psi_\alpha = E \mathbf{B}_{\alpha\beta} \psi_\alpha. \tag{37}$$

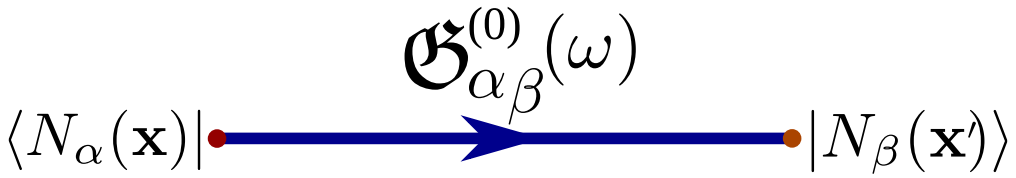

Figure 3: The notation for the lowest order propagator in a finite domain is shown. Here $\mathfrak{G}$ is the matrix operator for the propagator in the space of finite element global interpolation polynomials.

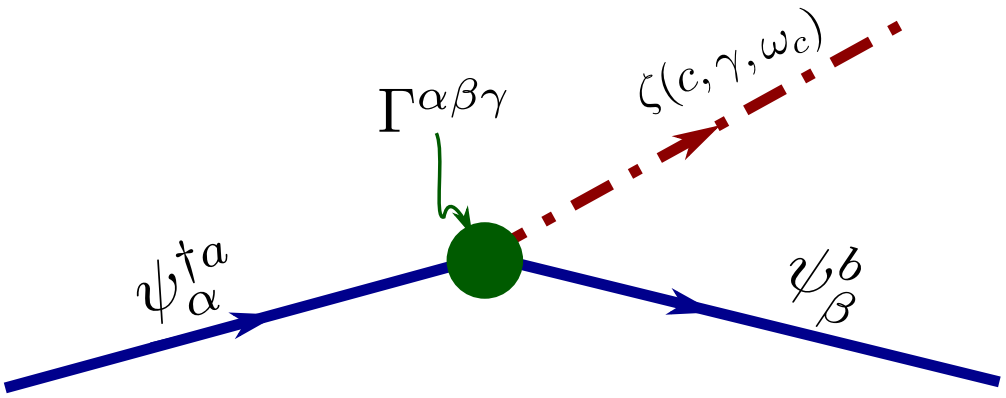

Figure 4: The first order phonon emission diagram is shown for a finite domain.

The matrices **K** and **V** are the 'kinetic' and potential energy terms, while **B** is the overlap matrix generated by the basis functions being not orthonormal.

Equation (37) is solved using standard methods for the eigenenergies and the corresponding nodal value array, of eigenfunctions, $(E_n, \psi_\alpha^{(n)})$. The full eigenfunctions are obtained by using the same interpolation polynomials used in the dicretization to reconstruct the wavefunction of the physical domain as in Eq. (35).

b The phonon emission process in a finite domain

The incoming electron has quantum numbers (a, s) while the outgoing electron has (b, s'). The emitted phonon has the quantum numbers (c, ω_c).The coupling is $\gamma = e$. The phonon field has a derivative coupling with the electrons, and its field is given by ζ. The Fröhlich interaction parameters are included in the factor Λ. The spatial integration using a finite element interpolated representation for all the fields is represented by $\Gamma^{\alpha\beta\delta}$. The coefficient vector arrays in the discretized representation of the wavefunction are in the factors $\psi^\dagger_\alpha$, ψ_β, and ζ_δ. For a particular incoming electron state labeled by (a, ω_a, s) going into an outgoing electron with quantum numbers (b, ω_b, s') and an LO-phonon with quantum numbers (c, ω_c) we have the matrix element for the transition given by

$$\begin{aligned}
\langle \psi_b; \zeta_c | S_{fi} | \psi_a \rangle &= \frac{-i}{\hbar} \left\{ \gamma \int d^3 r N_\alpha(\mathbf{r}) N_\beta(\mathbf{r}) N_\gamma(\mathbf{r}) \right\} \\
&\quad \times \left(\psi^{\dagger(a)}_\alpha \psi^{(b)}_\beta \zeta^{(c)}_\gamma \right) (2\pi) \delta(\omega_a - \omega_b - \omega_c) \\
&= \frac{-i}{\hbar} \Gamma^{\alpha\beta\gamma} . \left(\psi^{\dagger(a)}_\alpha \psi^{(b)}_\beta \zeta^{(c)}_\gamma \right) (2\pi) \delta(\omega_a - \omega_b - \omega_c). \qquad (38)
\end{aligned}$$

Here, we have specified all the quantum numbers of the incoming and outgoing states. To obtain the lifetime of a given discrete eigenstate, we have to sum over the available phase space (quantum numbers) for the discrete final states that contribute to the process in a manner consistent with energy conservation.

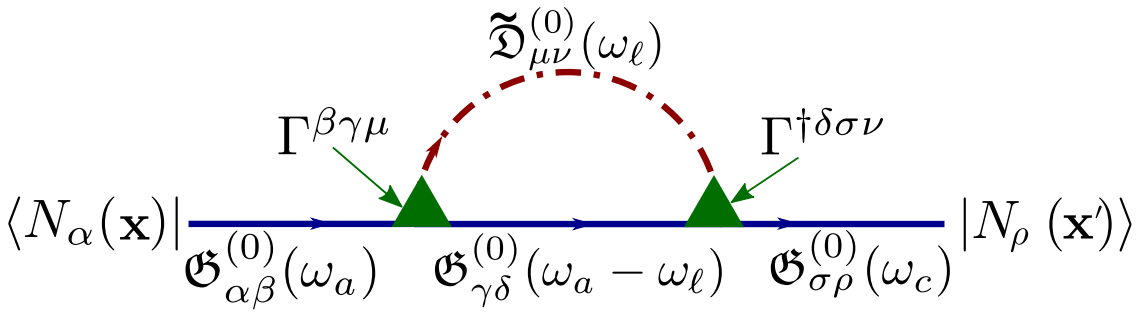

Figure 5: The second order propagator $G^{(2)}_{\alpha\beta}(\mathbf{x},\mathbf{x}',\omega)$ in a finite domain is shown in terms of the electron-phonon bubble diagram.

c Discretization of the lowest order propagators $G^{(0)}$ and $G^{(2)}$

The lowest order propagators, $G^{(0)}$ and $G^{(2)}$, for electrons are obtained within the finite element framework as described below.

We use Eqs. (6,35) in Eq. (8) to obtain

$$\begin{aligned} iG^{R(0)}(z,z',\omega) &= \sum_n \frac{\langle N_\alpha(\mathbf{z})|\left(\psi^n_\alpha \psi^{\dagger n}_\beta\right)|N_\beta(\mathbf{z})\rangle}{\omega-\omega_n+i\eta}, \\ &= \langle N_\alpha(\mathbf{z})|\mathfrak{G}^{R(0)}_{\alpha\beta}|N_\beta(\mathbf{z})\rangle. \end{aligned} \tag{39}$$

Observe that the interpolation polynomials are independent of n and the sum over the eigenstates can be cast purely in terms of the nodal parameters representing the eigenfunctions. Here the eigenstates are labeled by n, and α,β are the indices from the finite element discretization. The operator $\mathfrak{G}$ acts in the space of the nodal vectors, while the spatial dependence comes through the array of interpolation polynomials (shape functions) $N_\alpha(\mathbf{z})$ used in the discretization of the wavefunction. The numerator contains the direct product of two arrays

$$\mathfrak{F}^{(n)} = \psi^n_\alpha \otimes \psi^{\dagger n}_\beta \tag{40}$$

giving a matrix representing the corresponding field operator product in the usual propagator. Just as in the usual propagator we have a sum over intermediate states, here we have a sum over n in Eq.(39) and each intermediate state n gives rise to a matrix $\mathfrak{F}^{(n)}$ divided by the frequency denominator in the Green's function.

In practice, this sum over intermediate states can be truncated to go over only a few quantum numbers assuming the energy denominators lead to a desired error tolerance in the converging sum.

The notation for the discretized propagator $G^{(0)}$ is shown in the lowest order in Fig. 3. In the second order of perturbation we begin with Eq. (17). Employing the finite element form of the propagator Eq. (19), the integral over intermediate coordinates x_1, x_2 can be performed since the spatial dependence is again given by the interpolation polynomials. The integrals can be calculated on each element and then assembled over the global domain. The

eigenstates are labeled by lowercase letters $a, b, c, ...$ Let us define the vertex factor at z_2 in $G^{(2)}$ by $\mathbf{V}_{bcd}$,

$$\begin{aligned}\mathbf{V}_{bcd} &= \gamma \int d^3 z_2\, \psi^{\dagger(b)}(\mathbf{z}_2)\psi^{(c)}(\mathbf{z}_2)\, \zeta^{(d)}(\mathbf{z}_2) \\ &= \left\{\gamma \int d^3 z_2 N_\beta(\mathbf{z_2})N_\gamma(\mathbf{z_2})N_\delta(\mathbf{z_2})\right\}\left(\psi^{\dagger(b)}_\beta \psi^{(c)}_\gamma \zeta^{(d)}_\delta\right). \end{aligned} \tag{41}$$

The integral over the coordinate z_2 is independent of eigenvalue indices, and we write

$$\mathbf{\Gamma}_{\beta\gamma\delta} = \gamma \int dz_2 N_\beta(\mathbf{z_2})\, N_\gamma(\mathbf{z_2})\, N_\delta(\mathbf{z_2}). \tag{42}$$

The vertex $\mathbf{V}_{bcd}$ is then reduced to

$$\mathbf{V}_{bcd} = \mathbf{\Gamma}_{\beta\gamma\delta} \cdot \left(\psi^{\dagger(b)}_\beta \psi^{(c)}_\gamma \zeta^{(d)}_\delta\right). \tag{43}$$

Similarly, the second vertex at $\mathbf{z}_1$ in the one-loop diagram of Fig. 2 is given by

$$\begin{aligned}\mathbf{V}^\dagger_{pqs} &= \gamma \int d^3 z_1\, \psi^{\dagger(p)}(\mathbf{z}_1)\psi^{(q)}(\mathbf{z}_1)\, \zeta^{\dagger(s)}(\mathbf{z}_1) \\ &= \left\{\gamma \int dz_1 N_\lambda(\mathbf{z_1})\, N_\mu(\mathbf{z_1})\, N_\nu(\mathbf{z_1})\right\}\left(\psi^{\dagger(p)}_\lambda \psi^{(q)}_\mu \zeta^{\dagger(s)}_\nu\right) \\ &= \mathbf{\Gamma}^\dagger_{\lambda\mu\nu} \cdot \left(\psi^{\dagger(p)}_\lambda \psi^{(q)}_\mu \zeta^{\dagger(s)}_\nu\right). \end{aligned} \tag{44}$$

With the above results we obtain the propagator $G^{(2)}$ in terms of the nodal values and interpolation functions at zero temperature

$$\begin{aligned} iG^{(2)}(\mathbf{z}, \mathbf{z}', \omega) &= \frac{-1}{2\hbar^2}\int \frac{d\omega_1}{2\pi} \langle N_\alpha(z)| \Big\{ \\ &\quad \times \sum_a \left(\frac{\psi^{(a)}_\alpha \psi^{\dagger(a)}_\beta \theta(\omega_a - \omega_F)}{\omega - \omega_a + i\eta} - \frac{\psi^{(a)}_\alpha \psi^{\dagger(a)}_\beta \theta(\omega_F - \omega_a)}{\omega - \omega_a - i\eta} \right) \\ &\quad \times \Gamma^{\beta\gamma\mu} \sum_b \psi^{(b)}_\gamma \psi^{\dagger(b)}_\delta \left(\frac{\theta(\omega_b - \omega_F)}{\omega_1 - \omega_b + i\eta} - \frac{\theta(\omega_F - \omega_b)}{\omega_1 - \omega_b - i\eta} \right) \\ &\quad \times \sum_d \left(\frac{\zeta^{(d)}_\mu \zeta^{\dagger(d)}_\nu}{\omega - \omega_1 - \omega_d + i\eta} + \frac{\zeta^{(d)}_\mu \zeta^{\dagger(d)}_\nu}{\omega - \omega_1 + \omega_d - i\eta} \right) \Gamma^{\dagger\delta\sigma\nu} \\ &\quad \times \sum_c \Big(\frac{\psi^{(c)}_\sigma \psi^{\dagger(c)}_\rho \theta(\omega_c - \omega_F)}{\omega - \omega_c + i\eta} \\ &\qquad - \frac{\psi^{(c)}_\sigma \psi^{\dagger(c)}_\rho \theta(\omega_c - \omega_F)}{\omega - \omega_c - i\eta} \Big) \Big\} |N_\rho(\mathbf{z}')\rangle. \end{aligned} \tag{45}$$

The second order discretized propagator is shown in Fig. 5. This leads to

$$
\begin{aligned}
iG^{(2)}(\mathbf{z},\mathbf{z}',\omega) &= \langle N_\alpha(z)|\Bigg[\\
&\times \sum_a \left(\frac{\psi_\alpha^{(a)}\psi_\beta^{\dagger(a)}\theta(\omega_a-\omega_F)}{\omega-\omega_a+i\eta} - \frac{\psi_\alpha^{(a)}\psi_\beta^{\dagger(a)}\theta(\omega_F-\omega_a)}{\omega-\omega_a-i\eta} \right) \\
&\times \left\{ \Gamma^{\beta\gamma\mu} \left(\frac{-1}{2\hbar^2} \sum_{bd} \psi_\gamma^{(b)}\psi_\delta^{\dagger(b)}\zeta_\mu^{(d)}\zeta_\nu^{\dagger(d)} I_{bd} \right) \Gamma^{\dagger\delta\nu\sigma} \right\} \\
&\times \sum_c \left(\frac{\psi_\sigma^{(c)}\psi_\rho^{\dagger(c)}\theta(\omega_c-\omega_F)}{\omega-\omega_c+i\eta} - \frac{\psi_\sigma^{(c)}\psi_\rho^{\dagger(c)}\theta(\omega_F-\omega_c)}{\omega-\omega_c-i\eta} \right) \\
&\quad \Bigg] |N_\rho(\mathbf{z}')\rangle, \qquad (46)
\end{aligned}
$$

where I_{bd} is the two-pole integral

$$
\begin{aligned}
I_{bd} &= \int \frac{d\omega_1}{2\pi} \Bigg[\frac{-1}{(\omega_1-\omega_b+i\eta)(\omega_1-(\omega-\omega_d)-i\eta)} \\
&\quad + \frac{-1}{(\omega_1-\omega_b-i\eta)(\omega_1-(\omega+\omega_d)+i\eta)} \Bigg] \\
&= i\left[\frac{1}{(\omega-\omega_b-\omega_d)+i\eta} - \frac{1}{(\omega-\omega_b+\omega_d)-i\eta} \right]. \qquad (47)
\end{aligned}
$$

The step functions in Eq.(45) represent Fermi functions for particle creation above the Fermi level and hole creation below ω_F. The electron self-energy is identified easily, and we have

$$
\mathbf{\Sigma}_{\beta\sigma} = \Gamma^{\beta\gamma\mu} \left(\frac{i}{2\hbar^2} \sum_{bd} \psi_\gamma^{(b)}\psi_\delta^{\dagger(b)}\zeta_\mu^{(d)}\zeta_\nu^{\dagger(d)} I_{bd} \right) \Gamma^{\dagger\delta\nu\sigma} \qquad (48)
$$

Then, the real part of the self energy is given by

$$
\begin{aligned}
\mathrm{Re}\,\mathbf{\Sigma}_{\beta\sigma} &= \Gamma^{\beta\gamma\mu} \Bigg[\frac{-1}{2\hbar^2} \sum_{bd} \psi_\gamma^{(b)}\psi_\delta^{\dagger(b)}\zeta_\mu^{(d)}\zeta_\nu^{\dagger(d)} \\
&\quad \times \left(\frac{1}{\omega-\omega_b-\omega_d} - \frac{1}{\omega-\omega_b+\omega_d} \right) \Bigg] \Gamma^{\dagger\delta\nu\sigma}, \qquad (49)
\end{aligned}
$$

and the imaginary part is given by

$$
\begin{aligned}
\mathrm{Im}\,\mathbf{\Sigma}_{\beta\sigma} &= \Gamma^{\beta\gamma\mu} \Bigg\{ \frac{\pi}{2\hbar^2} \sum_{bd} \psi_\gamma^{(b)}\psi_\delta^{\dagger(b)}\zeta_\mu^{(d)}\zeta_\nu^{\dagger(d)} \\
&\quad \times [\delta(\omega-\omega_b-\omega_d) + \delta(\omega-\omega_b+\omega_d)] \Bigg\} \Gamma^{\dagger\delta\nu\sigma}. \qquad (50)
\end{aligned}
$$

The further developments of the above calculations will require explicit values for the wavefunction arrays.

5 Concluding remarks

.

We have developed the formalism in this article that allows us to use configuration space methods for quantum field theory calculations. A follow-up article will treat applications of quantum mechanics in realistic nanoscale structures.

We list below our finite element version of Feynman rules that are modified for finite domain quantum field theory and for quantum many-body systems:

1. Draw all the topologically distinct connected diagram. The total amplitude corresponds to the sum of all the diagrams.

2. For each incoming or outgoing Fermi line, include a factor corresponding to interpolation polynomial $N_\alpha(\mathbf{x}_i)$.

3. Assign a direction to each line to show the time flow, which determines the order of interpolation polynomials.

4. Each Fermion line corresponds to a factor

$$\mathfrak{G}^{(0)}_{\alpha\beta}(\omega) = \sum_a \frac{\psi^{(a)}_\alpha \psi^{\dagger(a)}_\beta}{\omega - \omega_a + i\epsilon}. \tag{51}$$

5. Each phonon line corresponds to a factor

$$\tilde{\mathfrak{D}}^{(0)}_{\mu\nu}(\omega_{l0}) = \sum_d \frac{\zeta^{(d)}_\mu \zeta^{\dagger(d)}_\nu}{\omega_{l0} - \omega_d + i\epsilon}. \tag{52}$$

6. Denote each electron phonon vertex by a triangle. Each vertex corresponds to a factor

$$\Gamma_{\beta\gamma\delta} \;\; = \;\; \gamma \int d^3x_j \, N_\beta(\mathbf{x}_j) N_\gamma(\mathbf{x}_j) N_\delta(\mathbf{x}_j), \tag{53}$$

   where γ represents the coupling coefficient e. Also, conserve energy at each triangle; affix a factor $(i/\hbar)^n$ where n is order of perturbation.

7. Integrate over internal energies.

We should mention that there are other equivalent methods to investigate quantum corrections, such as the functional methods espoused by Schwinger,[12–15] and the path-integral methods that are used in gauge field theory. We have confined ourselves to the Feynman diagram approach which allows a straightforward extension to finite domain field theory in real space through the use of Green's functions or Feynman propagators, in domains that have complex geometries, using FEM.

This extension developed by us goes beyond the usual treatment of layered nanoscale semiconductor structures or quantum dots in that we can investigate quantum phenomena in *arbitrarily shaped* 2D and 3D nanoscale systems. The FEM allows us to treat *arbitrary*

boundary conditions such as Dirichlet, Neumann, and mixed or Cauchy boundary conditions.[8]

The importance of LO-phonon and electron interactions are well appreciated. The electron self-energy due to LO-phonons,[16] and the consequent band-gap renormalization in wide-gap materials such as diamond is well documented.[17–21] In diamond, the estimated bandgap renormalization is $\sim 600\,\mathrm{meV}$, which is enormous. When we go from the infinite domain to finite systems, the boundary conditions alter the phonon spectrum[22] as well as the electronic states. The effective coupling constants are also altered. Thus, small structures of diamond can be expected to have different bandgap renormalization because the Fröhlich coupling between the L0-phonons with electrons will be altered by the presence of boundaries. Through the use of "cutting rules" of Landau and Cutkosky[23,24] we can connect the self-energy diagram calculation with the life-time calculation for the electron in phonon emission. In finite domains, we expect this carrier life-time estimate also to be altered and it can be readily calculated using the methods developed here.

We note that the "long-wavelength" phonon coupling to electrons is given by the usual Frölich coupling developed in the Appendices. The phonon coupling parameter actually varies with the momentum transferred to the phonon, and we have shown[25,26] that the coupling depends on the location of q in the Brillouin zone of the crystalline solid.

A Polar materials and phonons

The concept of the polaron was introduced by Landau[33,34] to describe an electron moving in a dielectric crystal. The crystal lattice is deformed due to the moving electron, thus creating a cloud of lattice vibrations around it known as the phonon cloud. This deformation of the lattice alters the mobility of the electrons thereby changing the effective mass. The polaron is a quasiparticle defined to be the electron coupled with its surrounding phonons in a polar material.[35]

For simplicity, the physical domain is assumed to be extended over the quantization volume V in this section, but the considerations presented here are readily adapted to the finite domain.[36,37] The electric polarization field

displacement $\mathbf{W} = \mathbf{u}\sqrt{M/V}$, where M is the reduced mass of the dipole in each unit cell and $\mathbf{u} = (\mathbf{u}_+ - \mathbf{u}_-)$ i s the atomic displacement that induces the polarization. We have the coupled equations[38–41]

$$\begin{aligned} \ddot{\mathbf{W}} &= -\omega_0^2 \mathbf{W} + b_{12}\mathbf{E}, \\ \mathbf{P} &= b_{21}\mathbf{W} + b_{22}\mathbf{E}. \end{aligned} \tag{54}$$

We can separate out the transverse and longitudinal parts of the ionic displacement to write $\mathbf{W} = \mathbf{W}_T + \mathbf{W}_\ell$ The transverse motion of ions does not produce a depolarization field. Hence

$$\ddot{\mathbf{W}}_T = -\omega_T^2 \mathbf{W}_T,$$

so that

$$\omega_0 = \omega_T.$$

The Maxwell displacement $\mathbf{D} = \mathbf{E} + 4\pi\mathbf{P} = \epsilon(\omega)\mathbf{E}$ allows us to relate $\mathbf{P}$ to the electric field. Furthermore, at high (optical) frequencies the ions cannot follow the electric field and hence

$$\mathbf{P}(\omega > \omega_{\rm opt}) = b_{22}\mathbf{E} = \frac{\epsilon_\infty - 1}{4\pi}\mathbf{E} \tag{55}$$

Hence

$$4\pi b_{22} = \epsilon_\infty - 1. \tag{56}$$

With a time dependence of $\exp(-i\omega t)$ for all fields we have

$$\ddot{\mathbf{W}}_\ell = -\omega_\ell^2 \mathbf{W}_\ell. \tag{57}$$

From Eqs. (54,56) we arrive at

$$\mathbf{P} = \left[b_{22} + \frac{b_{21}b_{12}}{(\omega_T^2 - \omega^2)} \right] \mathbf{E} = \frac{\epsilon(\infty) - 1}{4\pi}\mathbf{E}, \tag{58}$$

leading to

$$\begin{aligned} \epsilon(\omega) &= (1 + 4\pi b_{22}) + \frac{4\pi b_{21}b_{12}}{(\omega_T^2 - \omega^2)} \\ &= \epsilon_\infty + \frac{\epsilon_0 - \epsilon_\infty}{\omega_T^2 - \omega^2}\omega_T^2. \end{aligned} \tag{59}$$

This is the lattice dielectric function.[40,41]

If no electrons are present we would have

$$\nabla \cdot \mathbf{D} = 0 = \nabla \cdot (\mathbf{E} + 4\pi\mathbf{P}). \tag{60}$$

Substituting for $\mathbf{P}$ using Eq. (54) we have

$$\begin{aligned} \nabla \cdot \mathbf{E} &= -4\pi \nabla \cdot \mathbf{P} \\ &= -4\pi(b_{21}\nabla \cdot \mathbf{W}_\ell + b_{22}\nabla \cdot \mathbf{E}). \end{aligned}$$

Rearranging terms we obtain

$$\nabla \cdot \mathbf{E} = -\frac{1}{\epsilon_\infty} 4\pi b_{21} \nabla \cdot \mathbf{W}_\ell. \tag{61}$$

Since the electric field $\mathbf{E}$ and the ion displacement $\mathbf{W}_\ell$ are longitudinal, we conclude from the above that

$$\mathbf{E} = -\frac{4\pi b_{21}}{\epsilon_\infty}\mathbf{W}_\ell. \tag{62}$$

Combining Eqs. (54), (55), and (62) we have

$$\begin{aligned} \ddot{\mathbf{W}}_\ell &= -\omega_T^2 \mathbf{W}_\ell - \frac{4\pi b_{21}b_{12}}{1 + 4\pi b_{22}}\mathbf{W}_\ell \\ &= -\left(\omega_T^2 + \frac{(\epsilon_0 - \epsilon_\infty)\omega_T^2}{\epsilon_\infty} \right) \mathbf{W}_\ell \end{aligned} \tag{63}$$

leading to the Lyddane-Sachs-Teller[43] relation

$$\omega_\ell^2 = \omega_T^2 \, \frac{\epsilon_0}{\epsilon_\infty}. \tag{64}$$

In the presence of free electronic charges in the lattice the Maxwell displacement field satisfies the equation

$$\nabla \cdot \mathbf{D} = \nabla \cdot (\mathbf{E} + 4\pi \mathbf{P}) = 4\pi \rho_e. \tag{65}$$

Eliminating $\mathbf{P}$ using Eq. (54) we have

$$\nabla \cdot \mathbf{E} = -\frac{4\pi b_{21}}{\epsilon_\infty} \nabla \cdot \mathbf{W} + \frac{4\pi b_{21}}{\epsilon_\infty} \, \rho_e \tag{66}$$

The equation of motion for $\mathbf{W}$ now takes the form

$$\begin{aligned} \nabla \cdot \ddot{\mathbf{W}}_\ell &= -\omega_T^2 \nabla \cdot \mathbf{W}_\ell - \frac{4\pi b_{21} b_{12}}{1 + 4\pi b_{22}} \nabla \cdot \mathbf{W}_\ell + b_{12} \nabla \cdot \mathbf{E} \\ &= -\omega_\ell^2 \nabla \cdot \mathbf{W}_\ell + \frac{4\pi b_{12}}{\epsilon_\infty} \, \nabla \cdot \mathbf{E}_{vac}, \end{aligned} \tag{67}$$

by identifying $\nabla \cdot \mathbf{E}_{vac} = 4\pi \rho_e$. From energy considerations and reciprocity we have

$$b_{12} = b_{21} = \omega_T \sqrt{(\epsilon_0 - \epsilon_\infty)/4\pi}$$

and $\omega_T = \omega_\ell \sqrt{\epsilon_\infty / \epsilon_0}$, we can express the last term in Eq. (67) as arising from an interaction energy between the phonon field and the external charges.[38] We have

$$H_{\rm int} = -\frac{\omega_\ell}{\sqrt{4\pi}} \sqrt{\left(\frac{1}{\epsilon_\infty} - \frac{1}{\epsilon_0} \right)} \int d^3 r \, \mathbf{W}_\ell . \mathbf{E}_{vac}. \tag{68}$$

We note here that the Fröhlich coupling is treated as a constant defined in the long wavelength limit, or at the Γ-point in the Brillouin zone in the crystalline solid. This is a severe approximation. We have shown[25,26] that the coupling parameter in fact depends on the momentum transfer q to the phonon. We have used density functional theory to demonstrate that the coupling parameter depends strongly on q as it varies over the Brillouin zone.

a Quantization of the phonon field

The longitudinal optic phonon field $\mathbf{W}_\ell(\mathbf{r})$ couples to the electron. We begin from the Lagrangian density

$$\mathcal{L} = \frac{1}{2} \dot{\mathbf{W}}_\ell^2 - \frac{1}{2} \omega_\ell^2 \mathbf{W}_\ell^2 \tag{69}$$

The canonical momentum is then given by $\partial \mathcal{L} / \partial \dot{\mathbf{W}}_\ell = \dot{\mathbf{W}}_\ell$. The equal time commutation relation satisfied by the vector displacement field is

$$[W_i(\mathbf{r}), \, \dot{W}_j(\mathbf{r}')]_{t=t'} = i\hbar \delta^{(3)}(\mathbf{r} - \mathbf{r}') \delta_{ij}. \tag{70}$$

The longitudinal lattice displacement field $\mathbf{W}_\ell$ is assumed to be of the form[44]

$$\mathbf{W}_\ell(\mathbf{r},t) = \frac{\aleph}{\sqrt{V}}\sum_{\mathbf{k}}\frac{\mathbf{k}}{|\mathbf{k}|}\Big(e^{i\mathbf{k}\cdot\mathbf{r}-i\omega t}a_\ell(\mathbf{k}) + e^{-i\mathbf{k}\cdot\mathbf{r}+i\omega t}a_\ell^\dagger(\mathbf{k})\Big), \tag{71}$$

where $\aleph$ is the yet to be determined normalization factor. This normalization can be calculated using the commutation relation Eq. (70), which is a nonlinear relation in that the left side is bilinear in the field operators while the right side is not. Using the commutation relation between the creation and annihilation operators, $[a, a^\dagger] = 1$, we have

$$\begin{aligned}\Big[W_i(\mathbf{r},t),\, \dot{W}_j(\mathbf{r}',t)\Big] &= \sum_{\mathbf{k}\mathbf{k}'}\frac{\aleph_1\aleph_2}{V}\frac{k_i k_j'}{|\mathbf{k}||\mathbf{k}'|} \\ &\quad\times\Bigg[\Big(e^{i\mathbf{k}\cdot\mathbf{r}-i\omega t}a(\mathbf{k}) + e^{-i\mathbf{k}\cdot\mathbf{r}+i\omega t}a^\dagger(\mathbf{k})\Big), \\ &\quad i\omega'\Big(-e^{i\mathbf{k}'\cdot\mathbf{r}'-i\omega' t}a(\mathbf{k}')+e^{-i\mathbf{k}'\cdot\mathbf{r}'+i\omega' t}a^\dagger(\mathbf{k}')\Big)\Bigg] \\ &= \sum_{\mathbf{k}}\frac{\aleph_1\aleph_2}{V}\frac{k^2}{k^2}\Big(2i\omega_k e^{i\mathbf{k}\cdot(\mathbf{r}-\mathbf{r}')}\Big) \\ &= \sum_{\mathbf{k}}\frac{\aleph^2}{V}\Big(2i\omega_k e^{i\mathbf{k}\cdot(\mathbf{r}-\mathbf{r}')}\Big) \equiv i\hbar\delta^{(3)}(\mathbf{r}-\mathbf{r}').\end{aligned} \tag{72}$$

Here, despite being labelled differently, $\aleph_1$ and $\aleph_2$ are the same normalization factor and therefore can be rewritten as $\aleph$ in the final step. Comparing with Eq. (70), one obtains $\aleph = \sqrt{\hbar/(2\omega_k)}$, so that the quantized field is given by

$$\mathbf{W}_\ell(\mathbf{r},t) = \sum_{\mathbf{k}}\sqrt{\frac{\hbar}{2\omega_k V}}\frac{\mathbf{k}}{|\mathbf{k}|}\Big(e^{ik\cdot r}a_\ell(\mathbf{k}) + e^{ik\cdot r}a_\ell^\dagger(\mathbf{k})\Big), \tag{73}$$

where $(k\cdot r) = \mathbf{k}\cdot\mathbf{r} - \omega t$.

b The interaction Hamiltonian revisited

The interaction Hamiltonian, Eq. (68), can be cast in terms of quantized fields. Writing the electric field $\mathbf{E}_{vac}$ in terms of the gradient of the potential arising from the charge density we have

$$\mathbf{E}_{vac}(\mathbf{r}) = -\nabla_{\mathbf{r}}\int d^3r'\frac{e\,\psi_e^\dagger(\mathbf{r}')\psi_e(\mathbf{r}')d^3x'}{|\mathbf{r}-\mathbf{r}'|}. \tag{74}$$

The density of electrons is given by $\psi_e^\dagger\psi_e$. The electron field ψ_e is not specified further here, but will be expressed differently depending on the application. Using the vector identity $\nabla\cdot(\mathbf{A}\phi) = \phi\nabla\cdot\mathbf{A} + \mathbf{A}\cdot\nabla\phi$, the above expression can be rewritten as

$$H_I = \frac{-e\,\omega_\ell}{\sqrt{4\pi}}\left(\frac{1}{\epsilon_\infty}-\frac{1}{\epsilon_0}\right)^{1/2}\int d^3r'\psi_e^\dagger(\mathbf{r}')\psi_e(\mathbf{r}')\int d^3r\frac{\nabla_{\mathbf{r}}\cdot\mathbf{W}_\ell}{|\mathbf{r}-\mathbf{r}'|}. \tag{75}$$

Here, the surface term arising from Gauss's theorem is dropped since the energy is conserved. For the infinite domain the factor $1/|\mathbf{r}-\mathbf{r}'|$ can be Fourier expanded and the spatial integration with respect to $\mathbf{r}$ can be performed. This leads to

$$\begin{aligned}\int d^3r \frac{\nabla_{\mathbf{r}}\cdot\mathbf{W}_\ell}{|\mathbf{r}-\mathbf{r}'|} &= \sum_{\mathbf{q}}\frac{1}{(2\pi)^3}\int d^3k\int d^3r\frac{4\pi i|\mathbf{q}|^2}{k^2|\mathbf{q}|}\\ &\quad\times\sqrt{\frac{\hbar}{2\omega_q V}}e^{i\mathbf{k}\cdot(\mathbf{r}-\mathbf{r}')}\left(a_{\mathbf{q}}e^{i\mathbf{q}\cdot\mathbf{r}-i\omega t}-a^\dagger_{\mathbf{q}}e^{-i\mathbf{q}\cdot\mathbf{r}+i\omega t}\right)\\ &= \sum_{\mathbf{q}}\frac{4\pi i}{|\mathbf{q}|}\sqrt{\frac{\hbar}{2\omega_q V}}\left(a_{\mathbf{q}}e^{i\mathbf{q}\cdot\mathbf{r}'-i\omega t}-a^\dagger_{\mathbf{q}}e^{-i\mathbf{q}\cdot\mathbf{r}'+i\omega t}\right).\end{aligned}$$

Substituting the above equation into Eq. (75), we arrive at

$$\begin{aligned}H_I &= e\int d^3r'\psi^\dagger_e(\mathbf{r}')\psi_e(\mathbf{r}')\\ &\quad\times\Big[-i\sum_{\mathbf{q}}\frac{\sqrt{2\pi\hbar\omega_\ell(\mathbf{q})}}{i|\mathbf{q}|\sqrt{V}}\left(\frac{1}{\epsilon_\infty}-\frac{1}{\epsilon_0}\right)^{1/2}\left(a_{\mathbf{q}}e^{-iq\cdot r'}-a^\dagger_{\mathbf{q}}e^{iq\cdot r'}\right)\Big] \qquad (76)\\ &\equiv \gamma\int d^3r'\psi^\dagger_e(\mathbf{r}')\psi_e(\mathbf{r}')\zeta(\mathbf{r}').\end{aligned}$$

Here, the term in the square bracket is denoted by $\zeta(\mathbf{r}')$, and the coupling constant by $\gamma = e$. The field

$$\begin{aligned}\zeta(\mathbf{r}) &= -i\sum_q\sqrt{\frac{2\pi\hbar\omega_\ell}{V|q|^2}}\left(\frac{1}{\epsilon_\infty}-\frac{1}{\epsilon_0}\right)^{1/2}\left(a_q e^{i\mathbf{q}.\mathbf{r}-i\omega t}-a^\dagger_q e^{-i\mathbf{q}.\mathbf{r}+i\omega t}\right)\\ &= \sum_q\left(\Lambda\, a_q e^{i\mathbf{q}.\mathbf{r}-i\omega t}+\Lambda^* a^\dagger_q e^{-i\mathbf{q}.\mathbf{r}+i\omega t}\right) \qquad (77)\end{aligned}$$

is the effective field that represents the LO-phonon field in its coupling with the electron density. Here we have simplified the expression for $\zeta(\mathbf{r})$ by defining

$$\Lambda = -i\sqrt{\frac{2\pi\hbar\omega_\ell}{V|q|^2}}\left(\frac{1}{\epsilon_\infty}-\frac{1}{\epsilon_0}\right)^{1/2}. \qquad (78)$$

The stimulated emission of plasmon-polaritons using the above formalism is given in Ref.45 and Ref.46 in very narrow bandgap n-doped materials, such as $Hg_{1-x}Cd_xTe$ and $Pb_{1-x}Sn_xTe$.

c LO-phonon propagators

The longitudinal phonon propagator defined in the interaction picture takes the form[44]

$$iD^{(0)}_{ij}(x,x') = \langle 0|T\left(\hat{W}_{\ell,i}(x)\hat{W}_{\ell,j}(x')\right)|0\rangle. \qquad (79)$$

Fourier expanding the fields we have

$$iD_{ij}^{(0)}(x-x') = \frac{i}{(2\pi)^4}\int d^4k\, e^{-ip\cdot(x-x')} D_{ij}^{(0)}(k). \tag{80}$$

The propagator in frequency space can be written as

$$\begin{aligned} iD_{ij}^{(0)}(\mathbf{k},\omega) &= iV\left[\frac{\langle 0|\hat{W}_{l,i}(0)|n,\mathbf{k}\rangle\langle n,\mathbf{k}|\hat{W}_{l,j}(0)|0\rangle}{\omega-\omega_{n,\mathbf{k}}+i\eta}\right. \\ &\quad \left. -\frac{\langle 0|\hat{W}_{l,i}(0)|n,-\mathbf{k}\rangle\langle n,-\mathbf{k}|\hat{W}_{l,j}(0)|0\rangle}{\omega+\omega_{n,-\mathbf{k}}-i\eta}\right]. \end{aligned} \tag{81}$$

Using Eq. (73), each matrix element can be calculated as in the following

$$\langle 0|\hat{W}_{l,i}(0)|n,\mathbf{k}\rangle = \sqrt{\frac{\hbar}{2\omega_{\mathbf{k}}V}}\,\frac{k_i}{|\mathbf{k}|}.$$

Then the propagator can be written as[10,44]

$$\begin{aligned} iD_{ij}^{(0)}(\mathbf{k},\omega) &= \frac{i\hbar}{2\omega_k}\left(\frac{1}{\omega-\omega_{n,\mathbf{k}}+i\eta}-\frac{1}{\omega+\omega_{n,\mathbf{k}}-i\eta}\right)\frac{k_ik_j}{k^2} \\ &= \frac{i\hbar}{\omega^2-\omega_l^2(\mathbf{k})+i\eta}\,\frac{k_ik_j}{k^2}. \end{aligned} \tag{82}$$

The LO-phonon frequency is usually treated as being dispersionless; this is the typical approximation. The phonon propagator in intermediate states (bubble diagrams) can be simplified considerably by using the expression for $\zeta(\mathbf{r})$ given in Eq. (77). We can define

$$i\tilde{D}^{(0)}(r-r') = \langle 0|T\Big(\zeta(\mathbf{r})\zeta(\mathbf{r}')\Big)|0\rangle. \tag{83}$$

In momentum space we obtain

$$i\tilde{D}^{(0)}(\mathbf{q},\omega) = \left(\frac{4\pi\hbar\omega_\ell^2}{|q|^2}\right)\left(\frac{1}{\epsilon_\infty}-\frac{1}{\epsilon_0}\right)\frac{1}{(\omega^2-\omega_\ell^2+i\eta)}. \tag{84}$$

d LO-phonon propagators in finite domains

With a finite element representation for the phonon wavefunction $\zeta(r)$ we have

$$\zeta(\mathbf{r},t) = \sum_p\Big(\Lambda\, a_p\, N_\alpha(\mathbf{r})\zeta_\alpha^{(p)}e^{-i\omega_p t} + \Lambda^* a_p^\dagger\, N_\alpha(\mathbf{r})\zeta_\alpha^{\dagger(p)}e^{+i\omega_p t}\Big). \tag{85}$$

Here the index p refers to the phonon modes in the finite domain and the label α refers to the expansion of the wavefunction in terms of interpolatnarraylynomials N_α.

The phonon propagator in a finite system can be expressed in terms of the finite element representation of the wavefunctions using Eq. (85) . We have

$$\begin{aligned} i\tilde{D}^{(0)}(\mathbf{r},t;\mathbf{r}',t') &= \langle 0|T\Big(\zeta(\mathbf{r},t),\zeta^{\dagger}(\mathbf{r}',t')\Big)|0\rangle, \\ &= \theta(t-t')\langle 0|\Big(\zeta(\mathbf{r},t),\zeta^{\dagger}(\mathbf{r}',t')\Big)|0\rangle \\ &\quad +\theta(t'-t)\langle 0|\Big(\zeta^{\dagger}(\mathbf{r}',t'),\zeta(\mathbf{r},t)\Big)|0\rangle. \end{aligned} \tag{86}$$

We evaluate the matrix elements in the above equation and do a Fourier expansion in frequency to obtain

$$\begin{aligned} i\tilde{D}^{(0)}(\mathbf{r},\mathbf{r}',\omega) &= \sum_n \zeta_{\alpha}^{(n)} N_{\alpha}(\mathbf{r}) \zeta_{\beta}^{\dagger(n)} N_{\beta}(\mathbf{r}')|\Lambda|^2 \\ &\quad \times \int_0^{\infty} d(t-t') e^{i(\omega-\omega_n+i\eta)(t-t')} \\ &\quad + \sum_n \zeta_{\alpha}^{(n)} N_{\alpha}(\mathbf{r}) \zeta_{\beta}^{\dagger(n)} N_{\beta}(\mathbf{r}')|\Lambda|^2 \\ &\quad \times \int_{-\infty}^{0} d(t-t') e^{i(\omega+\omega_n-i\eta)(t-t')}. \end{aligned} \tag{87}$$

After some simplification we obtain

$$i\tilde{D}^{(0)}(\mathbf{r},\mathbf{r}',\omega) = \langle N_{\alpha}(\mathbf{r})|\Big(\sum_n |\Lambda|^2 \zeta_{\alpha}^{(n)} \zeta_{\beta}^{\dagger(n)} \frac{2\omega_n}{\omega^2-\omega_n^2+i\eta}\Big)|N_{\beta}(\mathbf{r}')\rangle. \tag{88}$$

Again, we can cast this relation in operator form by writing

$$\tilde{\mathfrak{D}}_{\alpha\beta}^{(0)}(\omega) = \sum_n \zeta_{\alpha}^{(n)} \zeta_{\beta}^{\dagger(n)} \frac{2\omega_n}{\omega^2-\omega_n^2+i\eta}. \tag{89}$$

We then have

$$i\tilde{D}^{(0)}(\mathbf{r},\mathbf{r}',\omega) = \langle N_{\alpha}(\mathbf{r})|\tilde{\mathfrak{D}}^{(0)_{\alpha\beta}}(\omega)|N_{\beta}(\mathbf{r}')\rangle. \tag{90}$$

e Fermion propagators

The free fermion field operator in Schrödinger's picture takes the form

$$\hat{\psi}(\mathbf{x}) = \sum_{\mathbf{k}\lambda} \psi_{\mathbf{k}\lambda}(\mathbf{x}) c_{\mathbf{k}\lambda}. \tag{91}$$

The $\mathbf{k}$, λ refer to wavevector and spin quantum numbers. The single free fermion GF is given by

$$iG_{\alpha\beta}^{(0)}(x,x') = \langle 0|T[\hat{\psi}_{\alpha}(x)\hat{\psi}_{\beta}^{\dagger}(x')]|0\rangle. \tag{92}$$

The subscripts α, β refer to spin quantum numbers. The coordinate x denotes $(\mathbf{x}, t)$. If the ground state is a many-electron state we denote this by replacing $|0\rangle$ by $|\Omega\rangle$. Since the particles can only be created to fill unoccupied states, above the Fermi sea, the free propagator is given by[9–11]

$$\begin{aligned} iG^{(0)}_{\alpha\beta}(x,x') &= \delta_{\alpha\beta}\sum_{\mathbf{k}} e^{i\mathbf{k}\cdot(\mathbf{x}-\mathbf{x}')}e^{-i\omega_k(t-t')} && (93)\\ &\quad\times[\theta(t-t')\langle\Omega|\hat{\psi}(0)|\mathbf{k}\rangle\langle\mathbf{k}|\hat{\psi}^{\dagger}(0)|\Omega\rangle && (94)\\ &\quad-\theta(t-t')\langle\Omega|\hat{\psi}^{\dagger}(0)|\mathbf{k}\rangle\langle\mathbf{k}|\hat{\psi}(0)|\Omega\rangle] && (95)\\ &= \delta_{\alpha\beta}V^{-1}\sum_{\mathbf{k}} e^{i\mathbf{k}\cdot(\mathbf{x}-\mathbf{x}')}e^{-i\omega_k(t-t')} && (96)\\ &\quad\times[\theta(t-t')\theta(k-k_F)-\theta(t-t')\theta(k_F-k)]. && (97)\end{aligned}$$

In the infinite domain, the summation over k becomes an integration, and V^{-1} is replaced by $(2\pi)^{-3}$. Similar to the phonon propagator, the free fermion propagator in momentum space is given by[9–11]

$$iG^{(0)}_{\alpha\beta}(\mathbf{k},\omega)=\delta_{\alpha\beta}\left(\frac{\theta(k-k_F)}{\omega-\omega(\mathbf{k})+i\eta}-\frac{\theta(k_F-k)}{\omega-\omega(\mathbf{k})-i\eta}\right). \tag{98}$$

In finite domains the spatial part of the wavefunctions have to be determined based on the geometry. In the finite element method, the wavefunction with quantum number n can be expressed as $\psi_n(\mathbf{r}) = \psi^{(n)}_{\alpha} N_{\alpha}(\mathbf{r})$. The wavefunctions expressed in terms of interpolation functions can be used in the Feynman propagators so that

$$\begin{aligned} iG^{(0)}(\mathbf{x},\mathbf{x}',\omega) &= \sum_a \Bigg[N_{\lambda}(\mathbf{x})\theta(n_a-n_F)\left(\frac{\psi^{\lambda}_a\psi^{\dagger\mu}_a}{\omega-\omega_a+i\eta}\right)N_{\mu}(\mathbf{x}')\\ &\quad -\theta(n_F-n_a)N_{\lambda}(\mathbf{x})\left(\frac{\psi^{\lambda}_a\psi^{\dagger\mu}_a}{\omega-\omega_a-i\eta}\right)N_{\mu}(\mathbf{x}')\Bigg]. \end{aligned} \tag{99}$$

Here the index a refers to the eigenstates that are summed over in representing the Green's function, the indices λ, μ are the nodal array of wavefunction values at the finite element nodes, and the interpolation polynomials are denoted with the same indices. The inclusion of many-body considerations is done through the use of Fermi distribution functions (step-functions at zero temperature). Each term in the sum over a represents a global matrix representation of the contribution of the corresponding eigenmode. The first term corresponds to the excitations above the Fermi level (electrons above the Fermi sea) so that $n_a > n_F$ and the second term with $n_F > n_a$ is for excitations below the Fermi level defined by the occupied states and corresponds to the contribution of holes to the Green's function. We can cast the sum in an operator form by writing

$$iG^{(0)}(\mathbf{x},\mathbf{x}',\omega) = \langle N_{\lambda}(\mathbf{x})|\mathfrak{G}^{(0)}_{\lambda\mu}(\omega)|N_{\mu}(\mathbf{x}')\rangle. \tag{100}$$

The Fermion distribution functions are incorporated into the operator for convenience. We are thus able to carry over all the concepts associated with the infinite domain into the nanoscale finite domain arena.

References

[1] R. P. Feynman, "Space-time approach to nonrelativistic quantum mechanics," Rev. Mod. Phys. **20**, 367–387 (1948).

[2] R. P. Feynman, "Space-time approach to quantum electrodynamics," Phys. Rev. **76**, 769–789 (1949).

[3] J. D. Bjorken and S. D. Drell, *Relativistic Quantum Mechanics* (Dover Publications, New York, 2013); *Relativistic Quantum Fields* (Dover Publications, New York, 2013).

[4] J. J. Sakurai, *Advanced Quantum Mechanics* (Addison-Wesley, New York, 1967).

[5] C. Itzykson and J. B. Zuber, *Quantum Field Theory* (McGraw-Hill, New York, 1980).

[6] M. E. Peshkin and D. V. Schroeder, *An Introduction to Quantum Field Theory* (Westview Press, New York, 1995).

[7] A. Zee, *Quantum Field Theory in a Nutshell* (Princeton University Press, Princeton, NJ, 2003).

[8] L. R. Ram-Mohan, *Finite Element and Boundary Element Applications in Quantum Mechanics*, (Oxford University Press, Oxford, UK, 2002).

[9] A. A. Abrikosov, L. P. Gorkov, and I. E. Dzyaloshinski, *Methods of Quantum Field Theory in Statistical Physics* (Dover, New York, 1969).

[10] G. D. Mahan, *Many-body Physics* (Plenum Press, New York, 1981).

[11] A. L. Fetter and J. D. Walecka, *Quantum Theory of Many-Particle Systems* (McGraw-Hill, San Francisco, 1971).

[12] J. Schwinger, "On gauge invariance and vacuum polarization," Phys. Rev. **82**, 664–679 (1951).

[13] J. Schwinger, "The theory of quantized fields. I," Phys. Rev. **82**, 914–927 (1951)

[14] P. C. Martin and J. Schwinger, "Theory of many-particle systems. I," Phys. Rev. **115**, 1342–1373 (1959)

[15] J. Schwinger, "Brownian motion of a quantum oscillator," J. Math. Phys. **2**, 407–432 (1961)

[16] G. Grimvall, *The Electron-Phonon Interaction in Metals* (North-Holland, New York, 1981).

[17] D. Olgun, M. Cardona, A. Cantarero, "Electron-phonon effects on the direct band gap in semiconductors: LCAO calculations," Solid State Communications **122**, 575589 (2002).

[18] M. Cardona, T. A. Meyer and M. L. W. Thewalt, "Temperature Dependence of the Energy Gap of Semiconductors in the Low-Temperature Limit," Phys. Rev. Lett. **92**, 196403–1–4 (2004).

[19] M. Cardona and M. L. W. Thewalt, "Isotope effects on the optical spectra of semiconductors," , Rev. Mod. Phys. **77**, 1173–1224 (2005).

[20] F. Giustino, M. L. Cohen, and S. G. Louie, "Electron-phonon interaction using Wannier functions," Phys. Rev. B **76**, 165108–1–19 (2007).

[21] F. Giustino, S. G. Louie, and M. L. Cohen, "Electron-phonon renormalization of the direct band gap of diamond," Phys. Rev. Lett. **105** 265501–1–4 (2010).

[22] N. Mori and T. Ando, "Electron-optical-phonon interaction in single and double heterostructure," Phys. Rev. B **40**, 6175-6188 (1989).

[23] L. D. Landau, "On analytic properties of vertex parts in quantum field theory," Nuclear Physics **13**, 181–192 (1959).

[24] R. E. Cutkosky, "Singularities and Discontinuities of Feynman Amplitudes," Journal of Mathematical Physics **1**, 429–433 (1960).

[25] N. Tandon, J. D. Albrecht, L. R. Ram-Mohan, "Electron-phonon coupling and associated scattering rates in diamond," Diamond and Related Materials **56**, 1-5 (2015).

[26] N. Tandon, J. D. Albrecht, L. R. Ram-Mohan, "Electron-phonon interaction and scattering in Si and Ge: Implications for phonon engineering," Journal of Applied Physics **118**, 1–6 (2015).

[27] S. Datta, *Electronic Transport in Mesoscopic Systems* (Cambridge University Press, Cambridge, 1995).

[28] P. Havu, V. Havu, M. J. Puska and R. M. Nieminen, "Nonequilibrium electron transport in two-dimensional nanostructures modeled using Greens functions and the finite-element method," Phys. Rev. B **69**, 115325–1–13 (2004).

[29] L. R. Ram-Mohan, K. H. Yoo, and J. Moussa., "The SchrdingerPoisson self-consistency in layered quantum semiconductor structures," Journal of applied physics **95**, 3081-3092 (2004).

[30] I. Vurgaftman, J. R. Meyer, L. R. Ram-Mohan, "Optimized second-harmonic generation in asymmetric double quantum wells," IEEE journal of quantum electronics 32 (8), 1334-1346 (1996).

[31] Lok C. Lew Yan Voon and L. R. Ram-Mohan, "Calculations of second-order nonlinear optical susceptibilities in III-V and II-VI semiconductor heterostructures," Physical Review B 50, 1442114434 (1994).

[32] L. R. Ram-Mohan and P. A. Wolff, "Energetics of acceptor-bound magnetic polarons in diluted magnetic semiconductors," Phys. Rev. B **38**, 1330-1339 (1988).

[33] L. D. Landau, "On the motion of electrons in a crystal lattice," Phys. Z. Sowjetunion **3** 664-665 (1933).

[34] L. D. Landau and S. I. Pekar, "Effective mass of a polaron," Zh. Eksp. Teor. Fiz. **18**, 419423 (1948) [in Russian], English translation: Ukr. J. Phys., Special Issue, **53**, p.71-74 (2008).

[35] H. Fröhlich, "Electrons in lattice fields", Adv. Phys. **3**, 325–361 (1954).

[36] J. T. Devreese and A. S. Alexandrov, *Advances in Polaron Physics* (Springer, Heidelberg, Germany, 2010).

[37] M. A. Stroscio and M. Dutta, *Phonons in Nanostructures* (Cambridge University Press, Cambridge, UK, 2005).

[38] M. Born and K. Huang, *Dynamical Theory of Crystal Lattices* (Clarendon Press, Oxford, UK, 1954).

[39] Kun Huang, "On the interaction between the radiation field and ionic crystals," Proc. Roy. Soc. (Lond) A **208**, 352–365 (1951).

[40] C. Kittel, *Introduction to Solid State Physics* (Wiley, New York, 1996).

[41] C. Kittel, *Quantum Theory of Solids* (J. Wiley, New York, 1963).

[42] N. W. Ashcroft and N. D. Mermin, *Solid State Physics* (Holt, Rinehart and Winston, New York, 1976).

[43] R. H. Lyddane, R. G. Sachs, and E. Teller, "On the polar vibrations of alkali halides," Phys. Rev. **59**, 673–676 (1941).

[44] L. R. Ram-Mohan, (unpublished notes); also see Ref.45 and Ref.46.

[45] H. Xie, L. R. Ram-Mohan and P. A. Wolff, "Electron-hole recombination in narrow-band-gap $Hg_{1-x}Cd_xTe$ and stimulated emission of LO phonons," Phys. Rev. B **42**, 3620–3627 (1990).

[46] R. B. Sohn, L. R. Ram-Mohan, H. Xie, and Peter A. Wolff, "Stimulated emission of LO phonons in narrow-band-gap semiconductors," Phys. Rev. B **42**, 3608–3619 (1990).